# ASSESSMENT OF THE BURNING-PLASMA OPERATIONAL SPACE IN ITER BY USING A CONTROL-ORIENTED CORE-EDGE MODEL WITH SOLPS PARAMETERIZATION

V. GRABER, E. SCHUSTER
Lehigh University
Bethlehem, Pennsylvania, United States of America
Email: graber@lehigh.edu

**Abstract**

For ITER operations, the range of desirable burning-plasma regimes with high fusion power output will be restricted by various operational constraints. These constraints include the saturation of ITER's heating and fueling actuators such as the neutral beam injectors, the ion and electron cyclotron heating systems, the gas puffing system, and the deuterium-tritium pellet injectors. Furthermore, the tritium concentration in the fueling lines could drift below its nominal value during long pulses. This could prevent the burning plasma's tritium content from being sufficiently replenished. In addition to these actuator constraints, the H-mode power threshold, divertor detachment, and the heat load on the divertor targets apply limitations to ITER's operational space. In this work, Plasma Operation Contour (POPCON) plots that map the aforementioned constraints to temperature-density space are used to investigate which constraints are most limiting towards accessing regimes with high fusion power output. The presented POPCON plots are based on a control-oriented core-edge model that couples the nonlinear density and energy response models for the core-plasma region with parameterized scalings for the edge-plasma regions (scrape-off-layer and divertor). These scalings were generated by parameterizing SOLPS simulation results of ITER with a tungsten divertor and impurity seeding (neon or nitrogen) in terms of the following core-plasma and actuator inputs: outflows of power and particles from the core-plasma region, the separatrix impurity concentration, the pumping speed, and the gas fueling rate. The output of these scalings include the influx particle from the edge-plasma region to the core-plasma region, the ion and electron separatrix temperatures, whether the divertor is in the detached regime, and the heat load on the divertor targets. With this control-oriented core-edge model, nonlinear burn controllers can be designed to meet burn control objectives in the core-plasma region while maintaining divertor detachment and safe heat loads on the divertor targets. Open-loop simulations illustrate the potential of the core-edge plasma model for burn control objectives.

## 1. INTRODUCTION

The development of sophisticated algorithms that can regulate a burning plasma's temperature and density, which is the purpose of burn control, will be crucial for ITER's success. A model-based approach to burn control design [1–3] is advantageous because it directly incorporates the nonlinear and coupled dynamics of the plasma system. Burn control is made more challenging due to the sensitivity of the core-plasma region to the edge-plasma regions and vice versa. For example, divertor detachment depends strongly on the particle density and the total power balance in the core-plasma region. Moreover, achieving burn control objectives and protecting the divertor target from melting will need to be carefully balanced because an increase in the fusion reaction rate intensifies the power flowing into the scrape-off-layer (SOL) and onto the divertor targets. The peak heat load on ITER's tungsten (W) divertor should remain below 10 MW/m$^2$ to avoid melting [4].

ITER will need to push against operational limits to access desirable plasma regimes that maximize the fusion power output. These operational limits not only include the maximum allowable heat load on the divertor targets but also the H-mode power threshold and the saturation of ITER's heating and fueling actuators. ITER's suite of actuators include two neutral beam injectors, ion and electron cyclotron heating systems, two pellet injectors, and a gas fueling system [5]. Nonlinear algorithms can make use of all of the aforementioned actuators to drive the plasma to regimes with desirable temperatures and densities. Desirable burning plasma regimes can be evaluated using POPCON (Plasma OPeration CONtour) plots [6] that map plasma conditions over temperature-density space. In prior work [7, 8], control-oriented plasma models were used to generate POPCON plots that studied how the aforementioned operational limits restrict the set of accessible burning plasma regimes (i.e., the ITER operable space). However, the plasma model used in [7] only considered the core-plasma region, and the differences between the model used in [8] and the model proposed in this work are briefly described below. In contrast, the study of the ITER operation window in [4, 9] was carried out using ASTRA, a high-fidelity core-transport code, with SOL-divertor scalings applied as boundary conditions.

A control-oriented model that couples the core region of burning deuterium-tritium (D-T) plasmas to the scrape-off-layer (SOL) and divertor regions is proposed in this work. It is anticipated that this model can aid in the development of nonlinear burn-control solutions and in the investigation of desirable burning plasma regimes for D-T ITER operations. In this model, the plasma's core region, which spans from the magnetic axis to the last-closed-flux-surface (LCFS), is governed by nonlinear response models for the plasma's density and temperature profiles. These models balance the transport of particles and heat coming in and out of the plasma's core. Meanwhile, the edge-plasma region, which extends beyond the LCFS, is governed by scaling laws that were generated by parameterizing the results of high-fidelity SOLPS4.3 simulations [9]. SOLPS4.3 is a sophisticated plasma boundary transport code package, and the parameterized simulations were carried out for high-power, D-T operations with a full-tungsten divertor. Furthermore, the edge-plasma region was assumed to be seeded with either neon or nitrogen impurities. In this work, the core-plasma model and the edge-plasma scaling laws are coupled through the exchange of various parameters. The scaling laws determine the particle influx across the separatrix (including D-T fuel) and the ion and electron separatrix temperatures that enter into the core-plasma model. The divertor target heat load and the degree of detachment are also determined by the scaling laws. These scaling laws depend on the power entering the SOL and the outflow of particles across the separatrix, which are determined by the core-plasma region's energy and density response models. For the purpose of control design, the core-plasma actuators are the auxiliary power and the pellet injection, and the edge-plasma actuators are the gas fueling and the particle pumping.

In prior work [8, 10], a core-SOL-divertor (CSD) model was developed by coupling the energy and density response models of the core-plasma region to a two-point model [11] of the SOL-divertor region (the model in [10] also included a neutral-particle response model for the divertor-plasma region). Similarly to the SOLPS4.3 parameterizations [9], the two-point model connects conditions at the separatrix to conditions near the divertor. In contrast to the model proposed in this work, the model in [10] relied on phenomenological quantities, such as the divertor retention time, which absorb many unknown relations (similarly to the global energy confinement time but without any widely used scaling laws that can be extrapolated to ITER and other future machines [12]). The values of these phenomenological quantities would have to be obtained by fitting the CSD model to either experimental data or transport simulations. By using parameterizations derived from high-fidelity SOL-divertor simulations of ITER, the model proposed in this work avoids this obstacle.

This paper is organized as follows. In Section 2, the proposed control oriented core-edge model is presented as a core-plasma model coupled to the aforementioned SOLPS4.3 parameterizations. Similarly to what was presented in [8, 10], Section 3 provides a simulation study that demonstrates how the proposed model can be used for integrated burn-divertor control design in addition to an assessment of the ITER operable space based on POPCON plots. Finally, conclusions are drawn and future work is proposed in Section 4.

## 2. THE CORE-EDGE BURNING PLASMA MODEL

The core-edge model presented in this section is illustrated in Fig. 1, and it couples nonlinear energy and density response models for the core-plasma region to scaling laws for the edge-plasma regions (the SOL and divertor). The domain of the core-plasma model is the confined plasma bounded by the separatrix, while the SOL-divertor scalings, which are taken from SOLPS4.3 parameterizations of ITER burning plasmas [9], define the boundary of the core-plasma model and conditions at the divertor target. For example, the energy and density response models for the core-plasma region depend the separatrix ion and electron temperatures and the influx of particles across the separatrix (excluding the pellet injection that enters directly into the core-plasma region), respectively. Meanwhile, the outflow of the power and particles across the separatrix and into the SOL are inputs to the SOL-divertor scalings.

Burn control and divertor protection algorithms can be designed independently from each other, but the sensitivity between the core and edge regions of the plasma makes an integrated approach more attractive. Using auxiliary heating, pellet injection, gas puffing and pumping, divertor-safe burn controllers based on the presented core-edge model can drive a plasma to regimes with high fusion reaction rates (which is an output of the core-plasma model), while protecting the divertor from dangerously high heat loads (which is an output out the SOL-divertor scalings). The core-plasma (orange) and edge-plasma (purple) variables in Fig. 1 are defined in Sections 2.1 and 2.2, respectively. Control algorithms should define the output of the actuators (magenta) in real-time during plasma operations. The presented model is designed to facilitate the synthesis of nonlinear controllers that use these actuators for integrated burn-divertor control.

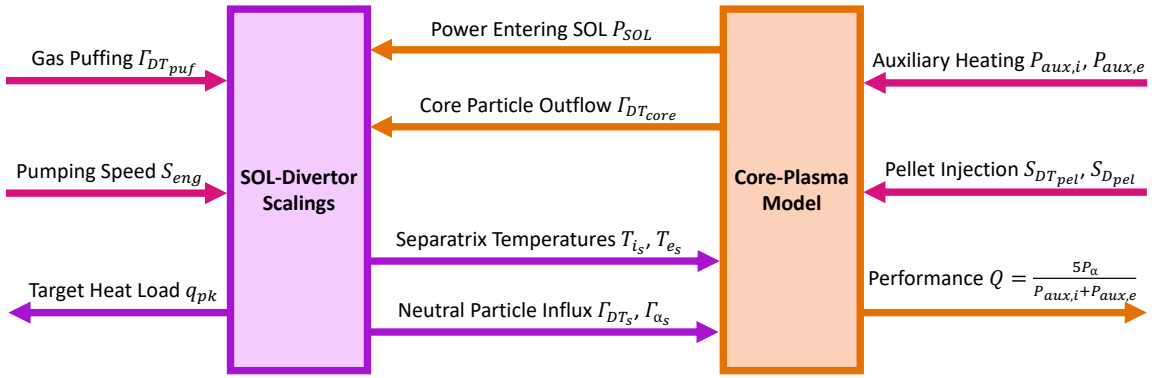


*FIG. 1. In the presented core-edge burning plasma model, the SOL-divertor scalings (purple) determine the peak heat load on the divertor targets, which must remain below a safety threshold to avoid catastrophic melting. In addition, the SOL-divertor scalings provide the following inputs to the core-plasma model: the ion separatrix temperature, the electron separatrix temperature, and the influx of particles (D, T, and $\alpha$) across the separatrix. The core-plasma model (orange) determines the performance of the burning plasma (e.g., the ratio between the fusion power and the auxiliary power) along with the following inputs to the SOL-divertor scalings: the power entering the SOL and the outflow of particles across the separatrix. The actuators (magenta) that enter into the SOL-divertor scalings are the gas fuel puffing and the pumping speed, whereas the auxiliary heating (e.g., neutral beam injection) and the pellet fuel injection enter into core-plasma model.*

### 2.1. The Core-Plasma Model

With each term in units of W/m$^3$, the volume-averaged ion energy ($E_i$) and electron energy ($E_e$) response models in the core-plasma region are given by,

$$\frac{d}{dt}E_i = -\frac{E_i}{\tau_{E,i}} + \phi_\alpha P_\alpha + P_{ei} + P_{aux,i}, \tag{1}$$

$$\frac{d}{dt}E_e = -\frac{E_e}{\tau_{E,e}} + (1-\phi_\alpha)P_\alpha - P_{ei} - P_{rad} + P_{ohm} + P_{aux,e}, \tag{2}$$

where $\phi_\alpha$ is the fraction of the alpha-particle power $P_\alpha$ that is deposited into the plasma's ion population, $P_{ei}$ is the collisional energy exchange between the ion and electron populations, $P_{rad}$ are the radiative losses, $P_{ohm}$ is the ohmic heating, and the ion and electron energies have a confinement time of $\tau_{E,i}$ and $\tau_{E,e}$, respectively. All of the terms in (1) and (2), except for the controlled external heating ($P_{aux} = P_{aux,i} + P_{aux,e}$) from ITER's various auxiliary heating sources, are dependent on the temperature of the plasma.

The ion and electron temperatures are assumed to have ITER-like parabolic profiles [13, 14]:

$$T_j(t,\psi) = (T_{j_0} - T_{j_s})(1-\psi/\psi_0)^2 + T_{j_s} \text{ for } j \in \{i,e\}, \tag{3}$$

where $\psi$ and $\psi_0$ are the toroidal magnetic flux coordinate and the total flux enclosed at the separatrix, respectively. For $j \in \{i,e\}$, the temperature profiles are defined by a peaked central temperature $T_{j_0}$ and a separatrix temperature $T_{s_0}$ (see Section 2.2). The volume average of (3) raised to the power $k$ is defined as

$$\langle T_j(t)^k \rangle = \frac{1}{\psi_0 - 0}\int_0^{\psi_0} [(T_{j_0} - T_{j_s})(1-\psi/\psi_0)^2 + T_{j_s}]^k d\psi \quad \text{for } j \in \{i,e\}. \tag{4}$$

The ion energy $E_i = \frac{3}{2}n_i\langle T_i\rangle$ and the electron energy $E_e = \frac{3}{2}n_e\langle T_e\rangle$ are dependent on the ion density $n_i$ and the electron density $n_e$, respectively. For $k = 1$, the solution of (4) is $\langle T_j\rangle = \frac{1}{3}T_{j_0} + \frac{2}{3}T_{j_s}$ for $j \in \{i,e\}$. In comparison to the parabolic temperature profiles, the profile of the total plasma density ($n = n_i + n_e$) in ITER is expected be relatively flat [11, 13, 14]. Thus, the approximation $n(t,\psi) \approx n(t)$ is made in this work (similarly to the POPCON study in [6]). The plasma consists of four different species: deuterium with density $n_D$, tritium with density $n_T$, alpha particles with density $n_\alpha$, and impurity particles with density $n_z$. Therefore, the ion density is $n_i = n_D + n_T + n_\alpha + n_z$. The quasi-neutrality condition (i.e., the number of electrons and protons in the plasma are equal) gives $n_e = n_D + n_T + 2n_\alpha + Z_z n_z$ where the impurity atomic number $Z_z$ is either $Z_{Ne} = 10$ for neon or $Z_N = 7$ for nitrogen.

Because each D-T fusion reaction produces an alpha particle with $Q_\alpha = 3.52$ MeV of kinetic energy, the alpha-particle power is $P_\alpha = f_{loss}Q_\alpha S_\alpha$ where $f_{loss}$ accounts for the percentage of alpha particles that escape confine-

ment before they are fully thermalized. The reaction rate density is $S_\alpha = n_D n_T \langle\sigma\nu\rangle$ where the D-T reactivity is calculated using the parameterizations presented in [15]:

$$\langle\sigma\nu\rangle = G(T_{i_0}) \times C_1 \omega \sqrt{\xi/(m_r c^2 T_{i_0}^3)} e^{-3\xi}, \tag{5}$$

$$\xi = (B_G^2/4\omega)^{1/3}, \qquad \omega = T_{i_0}\left[1 - \frac{T_{i_0}(C_2 + T_{i_0}(C_4 + T_{i_0}C_6))}{1 + T_{i_0}(C_3 + T_{i_0}(C_5 + T_{i_0}C_7))}\right]^{-1}. \tag{6}$$

The constants $m_r c^2$, $B_G$ and $C_j$ for $j \in \{1, ..., 7\}$ can be found in [15]. The correction factor $G(T_{i_0})$ from [6] is applied to account for the volume-averaging of the ion temperature profile.

In prior work [16], the following expression for the alpha power's ion-heating fraction [17, 18] was derived:

$$\phi_\alpha = \frac{1}{x_0}\left[\frac{1}{3}\ln\frac{1 - x_0^{1/2} + x_0}{(1 + x_0^{1/2})^2} + \frac{2}{\sqrt{3}}\Big(\arctan\frac{2x_0^{1/2} - 1}{\sqrt{3}} + \frac{\pi}{6}\Big)\right], \tag{7}$$

where $x_0 = \varepsilon_{\alpha_0}/\varepsilon_c$ is the ratio between the alpha particle's initial kinetic energy ($\varepsilon_{\alpha_0} = Q_\alpha$) and the critical energy $\varepsilon_c$. As an alpha particle loses energy from collisions with the surrounding particles in the plasma, less of its energy is transferred to the electrons and more of it is transferred to the ions. At the critical energy,

$$\varepsilon_c = m_e^{-1/3} A_\alpha \frac{\langle T_e\rangle}{n_e^{2/3}} \left(\frac{3\sqrt{\pi}\ln\Lambda_i}{4\ln\Lambda_e}\right)^{2/3} \left(\sum_{ions}\frac{n_i Z_i^2}{A_i}\right), \tag{8}$$

the alpha particle's kinetic energy is divided equally between the ions and electrons. In (8), the electron temperature is expressed in keV, $m_e = 9.1096 \times 10^{-31}$kg, the atomic mass is $A_\alpha = 4$, and the summation is taken over the plasma's four ion species (with $Z_D = Z_T = 1$ and $Z_\alpha = 2$). With the temperature expressed in K, the natural logarithm [19] is $\Lambda_k = 1.24 \times 10^7 \langle T_j^{3/2}\rangle/(n_e^{1/2} Z_{eff}^2)$ for $j \in \{i, e\}$ where the effective atomic number is given by $Z_{eff} = (Z_D^2 n_D + Z_T^2 n_T + Z_\alpha^2 n_\alpha + Z_z^2 n_z)/n_e$. For $k = \frac{3}{2}$, the solution of (4) is

$$\langle T_j^{3/2}\rangle = \frac{1}{4}T_{j_0}^{\frac{3}{2}} + \frac{3}{8}T_{j_s}\sqrt{T_{j_0}} + \frac{3}{8}\frac{T_{j_s}^2}{\sqrt{\Delta}}\ln(\sqrt{\Delta} + \sqrt{T_{j_0}}) - \frac{3}{8}\frac{T_{j_s}^2\ln\sqrt{T_{j_s}}}{\sqrt{\Delta}} \quad \text{for } j \in \{i, e\}, \tag{9}$$

where $\Delta = T_{j_0} - T_{j_s}$. The electron-heating fraction for $P_\alpha$ is $\bar{\phi}_\alpha = (1 - \phi_\alpha)$.

The losses due to bremsstrahlung radiation and the ohmic heating [17] are given by

$$P_{rad} = 5.5 \times 10^{-37} Z_{eff} n_e^2 \langle T_e^{1/2}\rangle, \tag{10}$$

$$P_{ohm} = 2.8 \times 10^{-9} Z_{eff} I_p^2 a^{-4} \langle T_e^{-3/2}\rangle, \tag{11}$$

where $T_e$ is expressed in keV, and the plasma current and minor radius for ITER [12] are $I_p = 15$ MA and $a = 2$ m, respectively. The solutions to (4) when $k = \frac{1}{2}$ and $k = -\frac{3}{2}$ are

$$\langle T_j^{1/2}\rangle = \frac{1}{2}\sqrt{T_{j_0}} + \frac{T_{j_s}}{2\sqrt{\Delta}}\ln\left|\frac{\sqrt{\Delta^2 + \Delta T_{j_s}} + \Delta}{\sqrt{\Delta T_{j_s}}}\right|, \tag{12}$$

$$\langle T_j^{-3/2}\rangle = \frac{1}{T_{j_s}\sqrt{T_{j_0}}} \quad \text{for } j \in \{i, e\}. \tag{13}$$

The collisional exchange of power between the ions and electrons [19] is given by

$$P_{ei} = \frac{3}{2}n_e\frac{\langle T_e\rangle - \langle T_i\rangle}{\tau_{ei}}, \qquad \tau_{ei} = \frac{3\pi\sqrt{2\pi}\varepsilon_0^2\langle T_e^{3/2}\rangle}{e^4 m_e^{1/2}\ln\Lambda_e}\sum_{ions}\frac{m_i}{n_i Z_i^2}, \tag{14}$$

where $e = 1.622 \times 10^{-19}$C and $\varepsilon_0 = 8.854 \times 10^{-12}$F/m. Similarly to the approaches taken in [6, 8], the volume average of $P_{ei}$ was approximated in (14).

With each term expressed in units of m$^3$/s, the deuterium (D), tritium (T) and alpha-particle ($\alpha$) densities have the following response models:

$$\dot{n}_D = -\frac{n_D}{\tau_D} - S_\alpha + (1 - \gamma)\Gamma_{DT_s} + C_{eff} S_{D_{pel}} + C_{eff}(1 - \gamma_{pel}) S_{DT_{pel}}, \tag{15}$$

$$\dot{n}_T = -\frac{n_T}{\tau_T} - S_\alpha + \gamma\Gamma_{DT_s} + C_{eff}\gamma_{pel} S_{DT_{pel}}, \tag{16}$$

$$\dot{n}_\alpha = -\frac{n_\alpha}{\tau_\alpha} + S_\alpha + \Gamma_{\alpha_s}, \tag{17}$$

where $\tau_D$, $\tau_T$ and $\tau_\alpha$ are particle confinement times, and $\gamma = n_T/(n_D + n_T) = n_T/n_{DT}$ is the tritium fraction of the plasma. The particle influxes coming from the edge-plasma region $\Gamma_{DT_s}$ and $\Gamma_{\alpha_s}$ are given in Section 2.2, and the outflow of fuel across the separatrix is $\Gamma_{DT_{core}} = (\frac{n_D}{\tau_D} + \frac{n_T}{\tau_T}) \times V$ where $V = 840$ m$^3$ is the ITER plasma volume [12]. The concentration of impurity particles in the core-plasma region is $c_{z_{core}} = n_z/n_e$ for $z \in \{\text{Ne}, \text{N}\}$. ITER is planned to be equipped with two pellet injectors. One of the injectors will be loaded with 100% deuterium pellets, while the other will be loaded with pellets that have a tritium fraction of $\gamma_{pel} = 90\%$. Respectively, the fuel rates of the two pellet injectors fuel are $S_{D_{pel}}$ and $S_{DT_{pel}}$. Because of the length of the guide tubes that will lead the pellets into the ITER vessel, the pellets are expected to lose approximately 10% of their mass ($C_{eff} = 90\%$) before entering the burning plasma [20].

The global energy confinement time for H-mode plasmas [12] is

$$\tau_E = 0.0562 H I_p^{0.93} R^{1.97} B^{0.15} M^{0.19} \epsilon^{0.58} \kappa^{0.78} n_e^{0.41} P_{tot}^{-0.69}, \tag{18}$$

$$P_{SOL} \equiv P_{tot} = (P_\alpha + P_{aux} - P_{rad} + P_{ohm}) \times V, \tag{19}$$

where $P_{SOL} \equiv P_{tot}$ is the power entering the SOL in MW, $H$ is the enhancement factor, $M = 3\gamma + 2(1-\gamma)$, and $n_e$ is in units of $10^{19}$ m$^{-3}$. For ITER, the toroidal magnetic field is $B = 5.3$ T, the plasma major radius is $R = 6.2$ m ($\epsilon = a/R$), the vertical elongation at the 95% flux surface is $\kappa = 1.7$. The confinement times for the particles, the ion energy and the electron energy are proportional to $\tau_E$: $\tau_D = k_D \tau_E$, $\tau_T = k_T \tau_E$, $\tau_\alpha = k_\alpha \tau_E$, $\tau_{E,i} = k_i \tau_E$ and $\tau_{E,e} = k_e \tau_E$ where $k_D$, $k_T$, $k_\alpha$, $k_i$ and $k_e$ are constants. When the total plasma power (19) exceeds the power threshold $P_{thresh}$ (MW), the plasma transitions from L-mode to H-mode [21]:

$$P_{thresh} = 4.3 M^{-1} B^{0.772} n_e^{0.782} R^{0.999} a^{0.975}. \tag{20}$$

### 2.2. The SOL-Divertor Scalings

In [9], SOLPS4.3 simulations were carried out to establish the following scalings for 60 MW $< P_{SOL} <$ 120 MW at $c_{z_{sep}} = 0.4\%$ and $c_{z_{sep}} = 1.2\%$, and also for $0.2\% < c_{z_{sep}} \leq 1.8\%$ at $P_{SOL} = 100$ MW where $c_{z_{sep}}$ for $z \in \{\text{Ne}, \text{N}\}$ is the seeded impurity concentration at the separatrix. This simulation study defined the parameter $\mu$ as the neutral pressure normalized to one at detachment:

$$\mu = \left( \frac{\Gamma_{DT_{SOL}}}{250 \bar{S}_{eng}} \right)^{0.83} \bar{P}_{SOL}^{-0.52}, \qquad (\mu \leq 1 \rightarrow \text{detached}), \tag{21}$$

where $\bar{P}_{SOL} = P_{SOL}$ [MW]/100, $\Gamma_{DT_{SOL}} = \Gamma_{DT_{core}} + \Gamma_{DT_{puf}}$ is the total D-T flux into the SOL (Pa m$^3$/s), $\Gamma_{DT_{core}}$ is given in Section 2.1, and $\Gamma_{DT_{puf}}$ is the controlled gas injection rate. The engineering pumping speed $S_{eng}$ (m$^3$/s) [22] is normalized to give $\bar{S}_{eng} = S_{eng}/57$. ITER's pumping system [5] can operate at speeds between 65 m$^3$/s and 107 m$^3$/s. The pumping speed can be modified in real-time, but the response time is slow (5–10 s).

The divertor heat load $q_{pk}$ (MW/m$^2$), which should remain below 10 MW/m$^2$ to avoid melting, is given by

$$\begin{bmatrix} q_{pk}|^{\text{Ne}} \\ q_{pk}|^{\text{N}} \end{bmatrix} = \max\left( \begin{bmatrix} 4.01 \\ 3.45 \end{bmatrix} \bar{P}_{SOL}^{1.44} \mu^{-0.83}, \quad 5.819 \bar{P}_{SOL}^{1.12} \mu^{-0.32} \begin{bmatrix} \bar{c}_{\text{Ne}_{sep}}^{-0.29} \\ \bar{c}_{\text{N}_{sep}}^{-0.19} \end{bmatrix} \right), \tag{22}$$

where $\bar{c}_{z_{sep}} = c_{z_{sep}}/0.004$ for $z \in \{\text{Ne}, \text{N}\}$. The electron and ion temperatures at the separatrix (eV),

$$\begin{bmatrix} T_{e_s}|^{\text{Ne}} \\ T_{e_s}|^{\text{N}} \end{bmatrix} = \bar{P}_{SOL}^{0.31} \left( \frac{\bar{P}_{SOL,e}}{\bar{P}_{SOL,i}} \right)^{0.05} \max\left( 140 \mu^{-0.093} \begin{bmatrix} \bar{c}_{\text{Ne}_{sep}}^{0.046} \\ \bar{c}_{\text{N}_{sep}}^{0.037} \end{bmatrix}, \quad 150 \begin{bmatrix} \bar{c}_{\text{Ne}_{sep}}^{0.092} \\ \bar{c}_{\text{N}_{sep}}^{0.063} \end{bmatrix} \right), \tag{23}$$

$$\begin{bmatrix} T_{i_s}|^{\text{Ne}} \\ T_{i_s}|^{\text{N}} \end{bmatrix} = \bar{P}_{SOL}^{0.27} \left( \frac{\bar{P}_{SOL,e}}{\bar{P}_{SOL,i}} \right)^{-0.13} \left( 1 + 0.08 \left( 1 - \frac{\Gamma_{DT_{puf}}}{\Gamma_{DT_{SOL}}} \right) \right)^{-1} \max\left( 200 \mu^{-0.19} \begin{bmatrix} \bar{c}_{\text{Ne}_{sep}}^{0.23} \\ \bar{c}_{\text{N}_{sep}}^{0.12} \end{bmatrix}, \quad 230 \bar{c}_{Z_{sep}}^{0.105} \right),$$

depend on $P_{SOL,e} = (1 - \phi_\alpha) P_\alpha + P_{ohm} - P_{rad} - P_{ei} + P_{aux,e}$ and $P_{SOL,i} \equiv \phi_\alpha P_\alpha + P_{ei} + P_{aux,i}$. The neutral particle fluxes across the separatrix (Pa m$^3$/s) for the DT fuel ($\Gamma_{DT_s}$) and He ($\Gamma_{\alpha_s}$) decrease with increasing $P_{SOL}$:

$$\begin{bmatrix} \Gamma_{DT_s}|^{\text{Ne}} \\ \Gamma_{DT_s}|^{\text{N}} \end{bmatrix} = \begin{bmatrix} \bar{c}_{\text{Ne}_{sep}}^{0.86} \\ \bar{c}_{\text{N}_{sep}}^{0.58} \end{bmatrix} \; 0.0053 \bar{P}_{SOL}^{-1.6} \mu^{-0.65} \bar{S}_{eng}^{-0.38} \Gamma_{DT_{SOL}} \left( 1 + 0.25 \left( 1 - \frac{\Gamma_{DT_{puf}}}{\Gamma_{DT_{SOL}}} \right) \right), \tag{24}$$

$$\Gamma_{\alpha_s} = 2 \bar{P}_{SOL}^{-1} \mu^{-0.33} \bar{c}_{Z_{sep}}^{0.35} \bar{S}_{eng}^{-0.93} \times (1.05 P_\alpha / P_{SOL}) \tag{25}$$

$$\times \max\left( 0.0016 \mu^{-1.9} \bar{c}_{Z_{sep}}^{-0.35}, \quad \min\left( \begin{bmatrix} 0.008 \\ 0.024 \end{bmatrix} \mu^{-0.46} \bar{c}_{Z_{sep}}^{-0.57}, \quad \begin{bmatrix} 0.0055 \\ 0.014 \end{bmatrix} \bar{P}_{SOL}^{1.18} \mu^{-1.42} \right) \right).$$

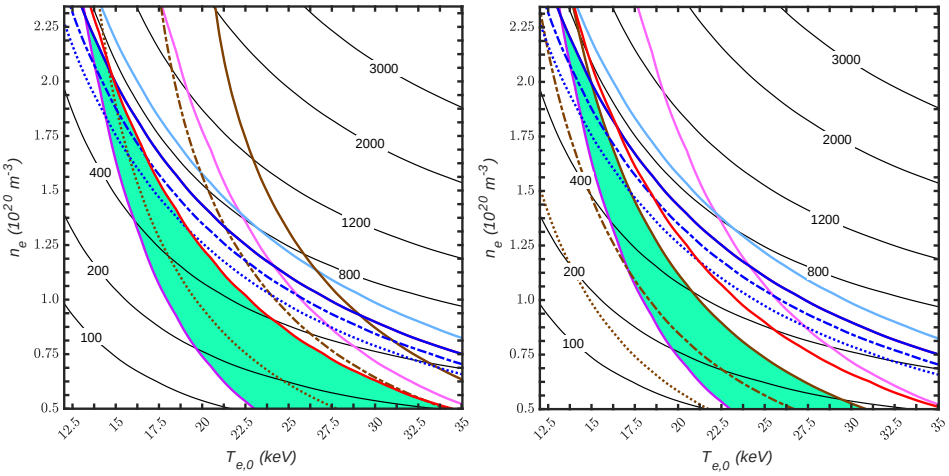


*FIG. 2. The left and right POPCON plots reveal steady-state conditions for ITER burning plasmas with a detached divertor ($\mu = 1$) and an attached divertor ($\mu = 1.4$), respectively. The solid black isolines map the fusion power in MW. The remaining solid isolines are operational limits: the auxiliary heating systems saturate (pink); the D pellet injector saturates (light blue); the D-T pellet injector saturates (dark blue); the gas fueling system saturates (brown); the divertor heat load exceeds the safety threshold (red); and the plasma is in H-mode (purple). The green area marks the space where all of the aforementioned operational limits are satisfied. Comparing the two plots, this green area in density-temperature space shrinks as the normalized divertor pressure $\mu$ increases.*

## 3. POPCON ASSESSMENT AND SIMULATION STUDY

The presented core-edge model enables the design of nonlinear controllers that can achieve burn-condition objectives while incorporating constraints dictated by safe divertor operation. For example, the plasma can be driven to high-power regimes while assuring that the heat load on the divertor is not too high. In this section, POPCON (Plasma Operation Contour) analysis based on this core-edge model reveals which steady-state plasma regimes are accessible to ITER under specific conditions. In addition, the usefulness of burn controllers synthesized from this control-oriented model is demonstrated with open-loop simulations.

Fig. 2 shows two POPCON plots that were generated from the presented control-oriented core-edge plasma model. These POPCON plots map the fusion power in MW (the solid black lines) over a wide range of core-plasma electron temperatures ($T_{e,0}$) and electron densities ($n_e$). In addition, contour lines for the following ITER operational constraints [5, 21, 23] are plotted: i- the auxiliary heating systems saturate at 110 MW (solid pink), ii- the 100%D pellet injector saturates at 120 Pa m$^3$/s (solid light blue), iii- the 10%D-90%T pellet injector saturates at 111 Pa m$^3$/s (solid dark blue), iv- the gas fueling system saturates (reaches peak throughput) at 400 Pa m$^3$/s (solid brown), v- the peak heat load on the divertor targets reaches the safety limit of 10 MW/m$^2$ (solid red), and vi- the total plasma power exceeds the L-H power threshold such that the plasma is in H-mode (solid purple). The region in temperature-density space where all six of the aforementioned constraints are satisfied is colored light green. This light green region indicates the operable space for the specific plasma plotted in the POPCON, and it reveals which constraints prevent access to plasma regimes with higher fusion powers.

In regard to pellet injection, the T concentration in the fueling lines, which can vary during long pulses, should remain high enough to replenish the T ion population and sustain the plasma's burn rate [3, 7]. Because adequate core-plasma T fueling is critical for ITER operations, additional saturation contour lines are shown (in Fig. 2) for the D-T pellet injector when the T concentration of the pellets are at 80% (dash-dot dark blue) and 70% (dotted dark blue). These additional contour lines show that the green operable space can shrink with decreasing T concentrations in the fueling lines. Also, additional contour lines are shown for when the gas fueling system's throughput is at 300 Pa m$^3$/s (dash-dot brown) and 200 Pa m$^3$/s (dotted brown).

The POPCON plots in Fig. 2 assume identical plasma conditions (e.g., both have a separatrix neon concentration of 0.4%) but different divertor conditions. The top plot assumes a detached divertor ($\mu = 1$), while the bottom plot assumes an attached divertor ($\mu = 1.4$). The maximum divertor heat load and the gas fueling saturation are the most restrictive constraints to the operable space of the detached and attached plasmas, respectively. The methodology for generating the POPCON plots is similar to that explained in prior work [7, 8], but the prior work did not consider the contribution of the gas injection to the plasma fueling and the divertor heat load mitigation.

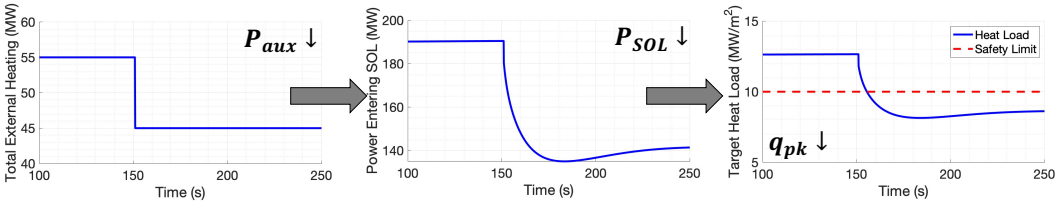


*FIG. 3. Decreasing the external heating lowers the amount of power entering the SOL, causing the divertor target heat load to fall below the safety limit.*

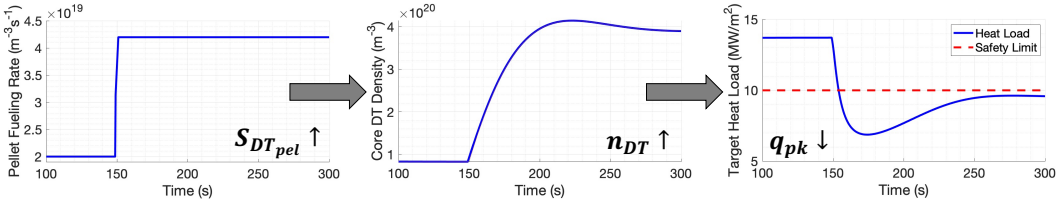


*FIG. 4. Increasing the injection rate of fuel pellets increases the deuterium-tritium density in the plasma's core. As a result, the divertor heat load falls below the safety limit.*

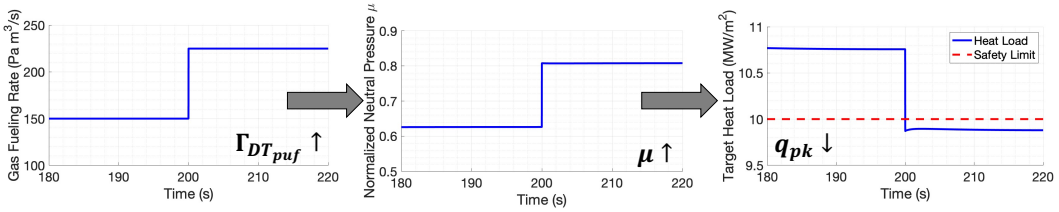


*FIG. 5. Increasing the gas puffing rate increases the normalized neutral pressure $\mu$, which causes the divertor heat load to drop below the safety limit.*

Nonlinear burn controllers designed using the presented core-edge model can employ ITER's various core-plasma actuators (e.g., neutral beam injection and pellet injection) to protect the divertor targets from high heat loads. In Fig. 3, the auxiliary heating ($P_{aux}$) is lowered to decrease the amount of power flowing into the SOL ($P_{SOL}$). Due to the positive correlation between $q_{pk}$ and $P_{SOL}$ in (22), the heat load on the divertor targets fall below 10 MW/m$^2$. In Fig. 4, the increased pellet injection rate ($S_{DT_{pel}}$) raises the fuel density ($n_{DT}$), which increases the outflow of fuel across the separatrix $\Gamma_{DT_{core}}$. The subsequent increase in $\Gamma_{DT_{SOL}} = \Gamma_{DT_{core}} + \Gamma_{DT_{puf}}$ increases divertor neutral pressure $\mu$ (21), which reduces the heat load $q_{pk}$ as governed by (22). In addition, controllers can employ edge-plasma actuators to regulate the divertor conditions. In Fig. 5, D-T gas puffing ($\Gamma_{DT_{puf}}$) into the SOL-divertor region is used to increase $\mu$ (by increasing $\Gamma_{DT_{SOL}}$), which decreases $q_{pk}$ accordingly (22). Algorithms can be designed to use these three actuators simultaneously for integrated burn-divertor control.

## 4. CONCLUSIONS AND FUTURE WORK

Burn control becomes more challenging once the divertor is taken into consideration because core-plasma and divertor-plasma objectives may conflict. For example, achieving higher fusion powers increases the power flowing into the SOL and intensifies the heat load on the divertor. In addition, increasing the impurity concentration at the separatrix reduces the heat load on the divertor, but it also pollutes the core of the plasma. The open-loop simulation results in Section 3 show how core-plasma and edge-plasma actuator systems can be utilized for integrated burn-divertor control. Because the presented control-oriented model couples the energy and density response models for the core-plasma region to SOLPS4.3 scalings [9] of the edge-plasma region, it can be used to synthesize nonlinear controllers that can achieve burn-control and divertor-control objectives simultaneously.

The POPCON analysis presented in this work gives insight how various operational constraints, such as actuator saturation and maintaining H-mode, render portions of the temperature-density space inaccessible to specific burning plasmas. For future work, a more comprehensive POPCON study can be undertaken to analyze changes to the operable space under a wide swath of parameter variations. For example, variations in the enhancement factor or the separatrix impurity concentration can be investigated.

## ACKNOWLEDGEMENTS

Work supported in part by the U.S. Department of Energy under DE-SC-0010661, and it was carried out in part under the ITER Scientist Fellow Network program.

## DISCLAIMER



## REFERENCES

[1] SCHUSTER, E., et al., Burn control in fusion reactors via nonlinear stabilization techniques, Fusion Sci. Technol. 43 (2002).

[2] BOYER, M., SCHUSTER, E., Nonlinear burn condition control in tokamaks using isotopic fuel tailoring, Nucl. Fusion 55 (2015).

[3] PAJARES, A., SCHUSTER, E., Robust nonlinear burn control in ITER to handle uncertainties in the fuel-line concentrations, Nucl. Fusion 59 (2019).

[4] PACHER, et al., ITER operation window determined from mutually consistent core–SOL–divertor simulations: definition and application, Nucl. Fusion 48 (2008).

[5] SNIPES, J., et al., Actuator and diagnostic requirements of the ITER Plasma Control System, Fusion Eng. Des. 87 (2012).

[6] MARTINELL, J., VITELA, J., An optimal burn regime in a controlled tokamak fusion power plant, IEEE Trans. Plasma Sci. 44 (2016).

[7] GRABER, V., SCHUSTER, E., Tritium-Concentration Requirements in the Fueling Lines for High-Q Operation in ITER, European Physical Society, Milan, Italy (2019).

[8] GRABER, V., SCHUSTER, E., Assessment of the burning-plasma operational space in ITER by using a control-oriented core-SOL-divertor model, Fusion Eng. Des. 171 (2021).

[9] PACHER, H., et al., Impurity seeding in ITER DT plasmas in a carbon-free environment, J. Nucl. Mater. 463 (2015).

[10] GRABER, V., SCHUSTER, E., Control-oriented core-SOL-divertor model to address integrated burn and divertor control challenges in ITER, Fusion Eng. Des. 192 (2023).

[11] STANGEBY, P., The Plasma Boundary, IOP, Bristol (2000).

[12] SHIMADA, M., et al., Chapter 1: Overview and summary, Nucl. Fusion 47 (2007).

[13] SHIMADA, M., et al., Physics design of ITER-FEAT, J. Plasma Fusion Res. 3 (2000).

[14] HARVEY, R., et al., Electron cyclotron heating and current drive in ITER, Nucl. Fusion 37 (1997).

[15] BOSCH, H., HALE, G., Improved formulas for fusion cross-sections and thermal reactivities, Fusion Sci. Technol. 52 (1992).

[16] GRABER, V., SCHUSTER, E., Nonlinear adaptive burn control and optimal control allocation of over-actuated two-temperature plasmas American Control Conference, Denver, USA (2020).

[17] WESSON, J., Tokamaks, 2nd ed., Clarendon Press, Oxford (1997).

[18] Gallart, D., Modelling of ICRF heating in DEMO with special emphasis on bulk ion heating, in AIP Conference Proceedings 1689 (2015).

[19] GROSS, R., Fusion Energy, Wiley-Interscience, New York (1984).

[20] COMBS, S., et al., Overview of recent developments in pellet injection for ITER, Fusion Eng. Des. 87 (2012).

[21] MARTIN, Y., et al., Power requirement for accessing the H-mode in ITER, J. Phys. Conf. Ser. 123 (2008).

[22] KUKUSHKIN, A., et al., Effect of the dome on divertor performance in ITER, J. Nucl. Mater. 363–365 (2007).

[23] LI, W., et al., A description of the ITER's gas injection systems and current R&D activities, Fusion Eng. Des. 87 (2012).